The development of new solar indices for use in thermospheric density modeling

W. Kent Tobiska*
Space Environment Technologies, Pacific Palisades, CA, 90272

S. Dave Bouwer†
Space Environment Technologies, Thornton, CO, 80260

and

Bruce R. Bowman‡
Air Force Space Command, Peterson AFB, CO, 80914

New solar indices have been developed to improve thermospheric density modeling for research and operational purposes. Out of 11 new and 4 legacy indices and proxies, we have selected three ($F_{10.7}$, $S_{10.7}$, and $M_{10.7}$) for use in the new JB2006 empirical thermospheric density model. In this work, we report on the development of these solar irradiance indices. The rationale for their use, their definitions, and their characteristics, including the ISO 21348 spectral category and sub-category, wavelength range, solar source temperature region, solar source feature, altitude region of terrestrial atmosphere absorption at unit optical depth, and terrestrial atmosphere thermal processes in the region of maximum energy absorption, are described. We also summarize for each solar index, the facility and instrument(s) used to observe the solar emission, the time frame over which the data exist, the measurement cadence, the data latency, and the research as well as operational availability. The new solar indices are provided in forecast (http://SpaceWx.com) as well as real-time and historical (http://sol.spacenvironment.net/~jb2006/) time frames. We describe the forecast methodology, compare results with actual data for active and quiet solar conditions, and compare improvements in $F_{10.7}$ forecasting with legacy HASDM and NOAA SEC forecasts.

Nomenclature

AU = *Astronomical Unit (measure of distance, 149 597 870 691 ±3 m)*
CME = *coronal mass ejection*
E_{SRC} = *145-165 nm solar irradiance index reported in $F_{10.7}$ units*
EUV = *extreme ultraviolet solar emissions ($10 \leq \lambda < 121$ nm)*
$F_{10.7}$ = *10.7-cm radio flux proxy for solar EUV in solar flux units (sfu) of $\times 10^{-22}$ W m^{-2} Hz^{-1}*
FUV = *far ultraviolet solar emissions ($122 \leq \lambda < 200$ nm)*
GPS = *Global Positioning Satellite system*
HASDM = *High Accuracy Satellite Drag Model*
HF = *High Frequency radio communication*
ISO 21348 = *International Standards Organization standard 21348 for determining solar irradiances*
JB2006 = *Jacchia-Bowman empirical thermospheric density model (2006)*
LEO = *Low Earth Orbit*
$M_{10.7}$ = *proxy for far ultraviolet solar irradiances between 145 – 165 nm reported in sfu*
MUV = *middle ultraviolet solar emissions ($200 \leq \lambda < 300$ nm)*
NOAA SEC = *National Oceanic and Atmospheric Administration Space Environment Center*
$S_{10.7}$ = *index for extreme ultraviolet solar irradiances between 26 – 34 nm reported in sfu*
S2K = *SOLAR2000 hybrid solar irradiance model*

* Chief Scientist, Space Environment Technologies Space Weather Division, 1676 Palisades Dr., Pacific Palisades, CA 90272; ktobiska@spacenvironment.net; http://SpaceWx.com; Senior AIAA member.
† Chief Engineer, Space Environment Technologies Space Weather Division, 986 Croke Dr., Thornton, CO, 80260.
‡ Scientist, Space Analysis A9AC, Air Force Space Command, Peterson AFB, CO, 80914; Bruce.bowman@peterson.af.mil; Senior AIAA member.

S_{EUV} = *26-34 nm solar irradiance index reported in $F_{10.7}$ units (same as $S_{10.7}$)*
SSA = *space situational awareness*
TEC = *Total Electron Content*
TRL = *Technology Readiness Level (1-9)*
UV = *ultraviolet solar emissions ($100 \leq \lambda < 400$ nm)*
X-rays = *X-ray solar emissions ($0.001 \leq \lambda < 10$ nm)*
XUV = *soft X-ray solar emissions ($0.1 \leq \lambda < 10$ nm)*
λ = *designator of solar spectral irradiance wavelength*

The Challenges of Space Weather

The near-Earth space environment contains abundant energy that affects natural and technological systems. The primary energy sources in the space environment come from dynamical processes related to stellar (including galactic), solar, and planetary (including comets, gas, and dust) evolution. The energy exists in the form of photons, particles (neutral and charged), and fields (magnetic, electric, and gravitational) and it is conserved, transferred, or exchanged. In addition to the natural photons, particles, and fields, human activity has added a new component to the near-Earth space environment, i.e., orbital debris. Together, these comprise the domain of the *near-Earth space environment* as shown in figure 1.

The short-term variable impact of solar photons, particles, and fields upon Earth's environment is known as *space weather*. These energy manifestations come from the interaction of solar magnetic phenomena with the solar surface and atmosphere. These phenomena include coronal holes, active regions, plage, and network and as well as flares and coronal mass ejections (CMEs). The result of these interactions is the collective production of energetic photons, electrons and protons. They make their way to Earth and affect our space-related technology through events such as single event upsets, latchup, surface charging, electrostatic discharge, high-frequency radio signal loss, polar cap absorption, scintillation, and atmospheric drag upon satellites.

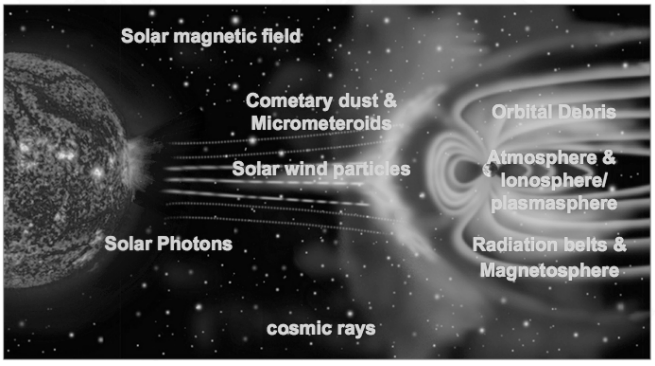

Fig. 1. Space environment components (photons, particles, fields) contribute to space weather (graphic credit NASA).

Accurate and precise orbit determination is complicated by perturbations upon satellite orbits caused by variable neutral atmosphere density and its drag against the spacecraft. Quantifying these density changes in the neutral atmosphere presents a special challenge and has been a topic of active research since the beginning of the space age. Natural density variations are controlled by two energy sources, i.e., primarily by direct solar irradiance photon illumination of and absorption by neutral species as well as secondarily by solar wind charged particles that interact with the magnetosphere and ionosphere system to create electric and magnetic fields responsible for subsequently heating the neutral atmosphere. The solar irradiances and solar wind drive the thermosphere-ionosphere-magnetosphere coupled system with a variety of characteristic forcing and relaxation response times. The response/relaxation times range from minutes to months. Therefore, understanding solar photon and particle forcing of the upper atmosphere is key to predicting the future neutral density state.

Because of the importance of space weather, there are substantive efforts underway to operationally characterize space weather as a coupled, seamless system from the Sun-to-Earth. This coupling links data streams and models to provide a capability for quantifying recent, current, and future conditions. In particular, advances in near-term operational forecasting have been made and we report on a major milestone accomplishment for mitigating space weather risks, i.e., the development of new solar irradiance indices with improved operational forecasts.

Rationale for New Solar Indices and Space Situational Awareness

Space situational awareness (SSA) has been described as the perception (measurement) of space environment elements within a volume of time and space, the comprehension (interpretation) of their meaning, and the projection (prediction) of their status into the near future. There are many space weather challenges to SSA including making observations, warnings, forecasts, and analyses with the accuracy, precision, resolution, and timeliness that are required to meet existing and future requirements. The requirements derive from classes of missions (communication, navigation, manned space, radar operations, satellite operations, debris monitoring, or surveillance) and there are

three common challenges between these classes: *making measurements rapidly, interpreting them quickly, and reacting to real-time and predicted information with appropriate and timely actions*. The capability we have developed that is described here will directly improve each of these mission classes by providing a fundamental technical capability that addresses those three challenges.

On-orbit and ground-components of space systems serve these mission classes and there are numerous examples of space weather effects upon them. Of immediate relevance are instrument or vehicle anomalies or catastrophic vehicle loss, loss of communications, increased in-space, in-air, on-ground navigation uncertainty, and vehicle or debris orbit change from drag effects. The improved solar irradiance capability we have developed mitigates space weather risks in each of these mission areas:

Communications: high frequency (HF) signal loss occurs from a change in the electron density profile and thus the reflecting layer of the ionosphere; this can lead to ground-to-ground and ground-to-air communication interruption or loss; it is a transient effect caused in low and mid latitudes by EUV photons during flares (minutes to hours);

Navigation: total electron content (TEC) variation occurs from a change in the integrated electron density and thus ionosphere column through which GPS signals pass from transmitter to receiver; this can lead to received signal timing error and thus position error in precision navigation systems; it is a transient effect caused in low and mid latitudes by EUV photons during flares (minutes to hours);

Orbital dynamics: satellite drag occurs at low Earth orbit (LEO) altitudes from density changes in the neutral thermosphere; this can lead to unmodeled in-track position error that affects satellite operations; it is particularly effective upon satellites without active propulsion and upon orbit debris particles of all sizes including re-entering vehicles; it is a cumulative effect caused in low and mid latitudes by EUV photons during solar active periods (hours to days).

We note that solar photons interacting with the neutral, then ionized, terrestrial atmosphere are common to these mission classes. The sources for these solar photons at all wavelengths are the magnetic field induced flare, active region, plage, network, and internetwork (background) radiance features that, summed together, form the full-disk solar irradiance as seen at 1 AU. We have made substantial progress in empirically characterizing how the photons will be effective at or near the Earth and predicting the irradiance fluxes with an accuracy and precision that meets current operational requirements. Our work is part of a coupled data–model system that is improving information content for operational systems in communication, navigation, manned space, radar operations, satellite operations, debris monitoring, and surveillance missions.

Definitions and ISO 21348 compliance

We utilize the new ISO 21348[1] (international standard for determining solar irradiances) definitions for solar spectral irradiance wavelength range designations and for distinguishing between solar irradiance indices and proxies. Solar spectral irradiance wavelength range designations are referred to in greater detail throughout this paper. Regarding solar irradiance indices and proxies, which are surrogates for solar irradiances, the usages of the terms are still evolving. A common usage is that a solar irradiance *proxy* is a measured or modeled data type that is used as a *substitute* for solar spectral irradiances. A solar irradiance *index*, on the other hand, is a measured or modeled data type that is an *indicator* of solar spectral irradiance activity level. Both can represent line, continua, and integrated irradiances or other irradiance-related solar features including an irradiance deficit from sunspots or sunspot numbers. Solar irradiance proxies and indices have quantifiable values related to solar processes and can be reported through a specified time interval. The new solar indices reported in this work are ISO 21348 Type 5 solar irradiance products for the ultraviolet and X-ray spectral categories. The process used for determining solar irradiances reported herein is compliant with *ISO International Standard 21348: Space environment (natural and artificial) – process for determining solar irradiances*.

The Selection and Development of New Solar Indices for Atmospheric Heating

We have studied, then developed, a variety of solar indices and proxies in order to characterize the solar energy absorbed in the atmosphere that leads to density changes observed by satellites. Table A summarizes these solar indices for atmospheric heating, their ISO 21348 spectral category, sub-category, wavelength range in units of nm, solar source temperature region, solar source feature, altitude region of terrestrial atmosphere absorption at unit optical depth in units of km, and terrestrial atmosphere thermal region of energy absorption. The indices and proxies marked with an asterisk (*) are those that have been selected for use in the modified Jacchia 1971 atmospheric density model, originally the CIRA72[2] model, that is described in companion papers and is now called the Jacchia-Bowman empirical thermospheric density model (JB2006)[3].

Table A. Solar indices studied for atmospheric heating

Index	ISO 21348[1] Spectral category	ISO 21348 Spectral sub-category	Wavelength range (nm)	Solar source temperature region	Solar source feature	Atmosphere absorption (unit optical depth, km)	Terrestrial atmosphere absorption (thermal region)
X_{hf}	X-rays	X-rays	0.1-0.8	Hot corona	Flare	70-90	Mesosphere
X_{b10}	X-rays	X-rays	0.1-0.8	Corona	Active region background	70-90	Mesosphere
$XE_{10.7}$	X-rays and UV	XUV+EUV	1-40	Chromosphere, corona	Active region, plage	90-200	Lower, mid thermosphere
$E_{10.7}$	X-rays and ultraviolet	XUV+EUV	1-105	Chromosphere, corona	Active region, plage, network	90-500	Thermosphere
*$F_{10.7}$	Radio	Radio	10.7E7	Transition region, cool corona	Active region	90-500	Thermosphere
*$S_{10.7}$	UV	EUV	26-34	Chromosphere, corona	Active region, plage, network	200-300	Thermosphere
$XL_{10.7}$	X-rays and UV	X-rays+H Lyman-α	0.1-0.8, 121	Chromosphere, transition region, corona	Active region, plage, network	70-90	Mesosphere
H Lya	UV	H Lyman-α	121	Transition region, chromosphere	Active region, plage, network	70-90	Mesosphere
E_{SRC0}	UV	FUV	125-175	Photosphere, chromosphere	Plage and network	90-125	Mesosphere, lower thermosphere
E_{SRC1}	UV	FUV	151-152	Chromosphere	Plage and network	125	Lower thermosphere
E_{SRC2}	UV	FUV	144-145	Chromosphere	Plage and network	125	Lower thermosphere
E_{SRC3} = E_{SRC}	UV	FUV	145-165	Photosphere, chromosphere	Plage and network	125	Lower thermosphere
*$M_{10.7}$	UV	MUV	280	Chromosphere	Active region	20	Stratosphere
E_{SRB}	UV	FUV+MUV	175-205	Photosphere	Plage and network	50-70	Mesosphere
E_{HRT}	UV	MUV	245-254	Photosphere	Network, background	25	Stratosphere

*Index or proxy is used in the JB2006[3] model exospheric temperature equation.

Table B. Characteristics of daily reported solar indices

Index or proxy	Observing facility	Instrument	Observation time frame	Measurement cadence	Measurement latency	Operational availability
$F_{10.7}$	Penticton ground observatory	Radio telescope	1947-2006	3 times/day	Up to 24 hours	yes
$S_{10.7}$	SOHO	SEM	1996-2006	15-second	Up to 24 hours	(a)
$XL_{10.7}$	GOES-12, UARS, SORCE, TIMED	XRS, SOLSTICE (2), SEE	1991-2006	1-minute, 16 times/day	Up to 10 minutes, up to 48 hours	(b)
E_{SRC}	UARS, SORCE	SOLSTICE (2)	1991-2006	16 times/day	Up to 48i hours	(c)
$M_{10.7}$	NOAA-16,17	SBUV	1991-2006	2 times/day	Up to 24 hours	yes
E_{HRT}	UARS, SORCE	SOLSTICE (2)	1991-2006	16 times/day	Up to 48 hours	(c)

(a) SOHO/SEM is a NASA research instrument but provides daily irradiances on an operational measurement cadence.
(b) GOES XRS is a NOAA operational instrument whereas TIMED/SEE and SORCE/SOLSTICE are NASA research instruments providing daily irradiances on an operational measurement cadence.
(c) UARS/SOLSTICE stopped in 2005; SORCE/SOLSTICE intends to provide data for several years.

In selecting candidate solar indices for driving the thermospheric densities, we first considered the altitudes of unit optical depth for solar photon energy deposition across a variety of wavelengths. Figure 2 demonstrates, in a simplified form, the range of unit optical depths we considered by altitude, wavelength, and absorbing species. It became apparent that previous models using $F_{10.7}$ as a solar proxy were primarily considering the heating of atomic oxygen above 180 km by the EUV solar photons. Other wavelengths in the XUV, X-rays, Lyman-α, and FUV were not included in empirical modeling formulations. Therefore, our first objective was to correct the missing solar heating by adding a component in the FUV that deposits energy in the lower thermosphere and that is centered on the Schumann-Runge continuum near 150 nm. We additionally considered other mesosphere/lower thermosphere (50-70, 90-125 km) heating processes as well as stratospheric (20–40 km) heating. The results, after removing known effects from the JB2006[3] model and modeling the residuals with the additional solar emissions, are briefly discussed below as well as more fully in Bowman and Tobiska[4].

The daily indices considered in detail, including their source, development, and formulation, were the $F_{10.7}$, $S_{10.7}$ (or S_{EUV}), $M_{10.7}$, $XL_{10.7}$, E_{SRC}, and E_{HRT}. The solar proxies or indices all exist through the common time frame of January 1, 1996 through June 12, 2005. Our methodology was to develop each index or proxy (Tables A and B) and validate it against the data used to derive it. The index or proxy was then used as an input into the JB2006[3] atmos-

pheric density model prototype with least squares best-fit time lag and within a multiple linear regression formulation as described in Bowman and Tobiska[4]. The resulting densities were compared with 18 known satellites' derived density data over the same time frame. After analyzing the residual error between the modeled and satellite-derived densities, and considering other factors such as operational availability of the index or proxy, only the $F_{10.7}$, $S_{10.7}$, and $M_{10.7}$ indices, along with their 81-day centered smoothed values, were selected for use in JB2006[3]. We studied many different smoothing schemes, both centered and backward smoothing over a multiplicity of time frames but found that the 81-day centered smoothing with the moving box-car method produced the lowest residuals in our modeled versus derived densities. We describe our results here.

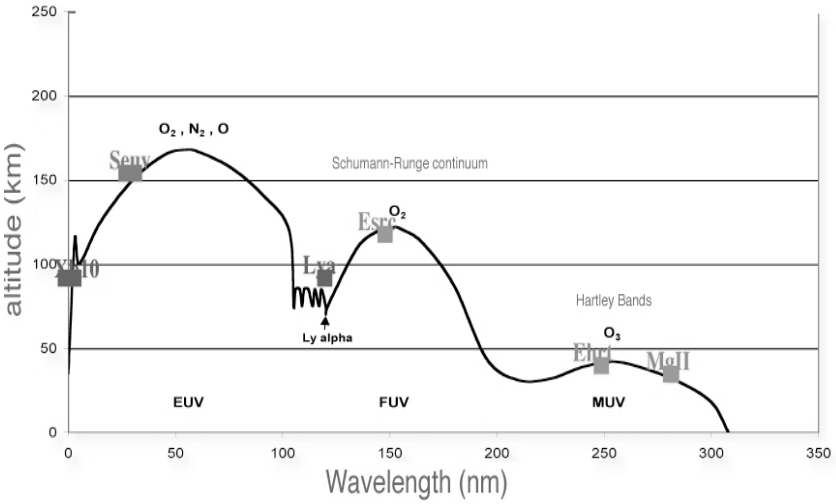

Fig. 2. Unit optical depth (altitude of maximum heating) for solar irradiances ranging from X-ray to MUV wavelengths. Neutral species that participate in heating are labeled in black and index designator for selected bandpasses are shown in gray.

$F_{10.7}$: The 10.7-cm solar radio flux, $F_{10.7}$, was first observed by Covington[5] on a daily basis beginning on February 14, 1947 and is now produced daily by the Canadian National Research Council's Herzberg Institute of Astrophysics at its ground-based Dominion Radio Astrophysical Observatory located in Penticton, British Columbia. Observations of the $F_{10.7}$ flux density values are made at 18, 20 and 22 UT each day and made available through the DRAO website http://hia-iha.nrc-cnrc.gc.ca/drao/icarus_e.html. The 20 UT values are archived at the World Data Center and were used in this study. The physical units of $F_{10.7}$ are $\times 10^{-22}$ W m^{-2} Hz^{-1} and we use the numerical value without the multiplier as is customarily done and expressed as solar flux units (sfu). In other words, a 10.7-cm radio emission of 150×10^{-22} W m^{-2} Hz^{-1} is simply referred to as $F_{10.7} = 150$ sfu.

We have created a running 81-day centered smoothed set of values using the moving box-car method and these data are referred to as either F_{81} or F_{BAR}. In our analysis, we have used linear regression with daily $F_{10.7}$ to scale and report all other solar indices in units of sfu. Missing data values are not included in the regressions.

$F_{10.7}$ is the traditional solar energy proxy that has been used since Jacchia developed empirical exospheric temperature equations for atmospheric density models, e.g., CIRA72. It's formation is physically dominated by non-thermal processes in the solar transition region and cool corona and, while it is a non-effective solar emission relative to the Earth's atmosphere, it is a useful proxy for the broad combination of chromospheric, transition region, and coronal solar EUV emissions modulated by bright solar active regions whose energy, at Earth, is deposited in the thermosphere. We use the observed archival daily values, with a 1-day lag, over the common time frame as described in Bowman and Tobiska[4].

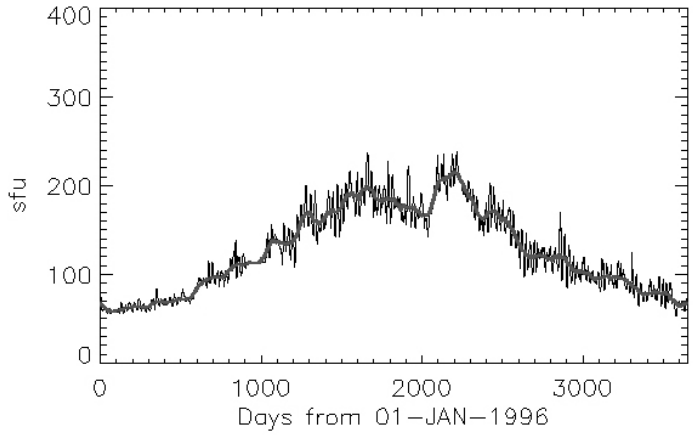

Fig. 3. $S_{10.7}$ shown in black from 1996 into 2005 in sfu and 81-day centered smooth shown in black bold.

$S_{10.7}$: The NASA/ESA Solar and Heliospheric Observatory (SOHO) research satellite operates in a halo orbit at the Lagrange Point 1 (L1) on the Earth-Sun line, approximately 1.5 million km from the Earth, and has an uninterrupted view of the Sun. One of the instruments on SOHO is the Solar Extreme-ultraviolet Monitor (SEM) that was built and is operated by University of Southern California's (USC) Space Science Center (SSC). SOHO was launched on December 2, 1995 and SEM has been making observations since December 16,

1995. As part of its continuous solar observations, the SEM instrument measures the 26–34 nm solar EUV emission with 15-second time resolution in its first order broadband wavelength range. The orbit and solar data are both retrieved daily by USC SSC for processing in order to create daily solar irradiances with a latency of up to 24 hours as described by Judge, *et al* [6].

We have used the integrated 26–34 nm emission ($SOHO\_SEM_{26\text{-}34}$) and normalized it by dividing the daily value by the common time frame mean value. The $SOHO\_SEM_{26\text{-}34mean}$ mean value is 1.9955×10^{10} photons cm^{-2} s^{-1}. The normalized value is converted to sfu through linear regression with $F_{10.7}$ over the common time frame and the resulting index is called S_{EUV}. Equation 1 is the formulation to derive the SOHO EUV, S_{EUV}. Figure 3 shows the S_{EUV} index ($S_{10.7}$) and the S_{81} (81-day centered smoothed) values for 1996 into 2005 during the common time frame.

The broadband (wavelength integrated) SEM 26-34 nm irradiances, represented by the $S_{10.7}$ index, are EUV line emissions dominated by the chromospheric He II line at 30.4 nm with contributions from other chromospheric and coronal lines. This energy principally comes from solar active regions, plage, and network. Once the photons reach the Earth, they are deposited (absorbed) in the terrestrial thermosphere mostly by atomic oxygen above 200 km. We use the daily index, with a 1-day lag, over the common time frame as described in Bowman and Tobiska[4].

$$S_{10.7} = (-12.01) + (141.23) \times (SOHO\_SEM_{26\text{-}34}/SOHO\_SEM_{26\text{-}34mean}) \quad (1)$$

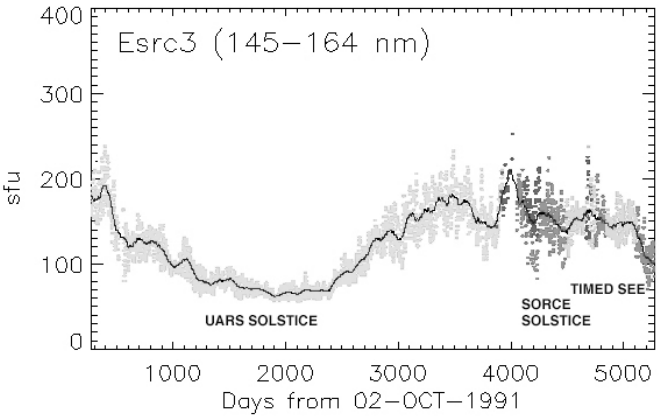

Fig. 4. E_{SRC} shown from 1991 into 2005 in sfu and 81-day centered smooth shown in black.

E_{SRC}: The solar FUV Schumann-Runge Continuum (SRC) contains emission between 125–175 nm from the photosphere and lower chromosphere. This solar energy is deposited in the terrestrial mesosphere and lower thermosphere (80–125 km) primarily through the energy released from the dissociation of molecular oxygen.

The SRC has been observed with the SOLSTICE instruments on UARS by Rottman and Woods[7] and on SORCE by McClintok, *et al.*[8] These are NASA research satellites as is the TIMED satellite that hosts the SEE instrument (Woods, *et al.*[9]); all three are conducting long-term investigations of solar spectral irradiances. After a comparison of three bands in the SRC (144–145, 151–152, 145–165 nm), we selected the 145–165 nm band (E_{SRC3} in Table A) as a representative wavelength range for the remainder of the SRC. The emission in this band is mostly deposited in the 110–125 altitude region.

In order to conduct our analysis, we integrated the daily SOLSTICE 145–165 nm emission from UARS and SORCE, created a normalized index by dividing the daily value by the common time frame mean value, $SOLSTICE_{145\text{-}165\text{-}mean}$, which has a value of 2.1105×10^{11} photons cm^{-2} s^{-1}. Next, we performed a linear regression with $F_{10.7}$ to report the index in sfu. E_{SRC}, as shown in equation 2, is the result and we used this index with a 5-day lag. Figure 4 shows the E_{SRC} and the E_{SRC81} (81-day centered smoothed) values as the combination of UARS, TIMED, and SORCE data.

$$E_{SRC} = (-784.03) + (909.34) \times (SOLSTICE_{145\text{-}165}/SOLSTICE_{145\text{-}165\text{-}mean}) \quad (2)$$

E_{HRT}: The solar MUV Hartley Band (HB) contains emission between 245–254 nm from the photosphere. This solar energy is deposited in the terrestrial stratosphere (30–40 km) primarily through the energy released from the dissociation of ozone. The solar HB emissions have been observed daily by the SOLSTICE instrument on the UARS and SORCE NASA research satellites.

For our analysis, we have integrated the daily SOLSTICE 245–254 nm emission and created a normalized index by dividing the daily value by the common time frame mean value, $SOLSTICE_{245\text{-}254\text{-}mean}$, which has a value of 3.1496×10^{13} photons cm^{-2} s^{-1}. Next, we performed a linear regression with $F_{10.7}$ to report the index in sfu. E_{HRT}, as shown in equation 3, is the result and we have used this index with multiple-day lags but with no apparent effect upon reducing the JB2006[3] modeled residuals with respect to the satellite-derived density data.

$$E_{HRT} = (-726.27) + (851.57) \times HB_{245\text{-}254}/HB_{245\text{-}254\text{-}mean} \quad (3)$$

$M_{10.7}$: The NOAA series operational satellites, e.g., NOAA 16 and NOAA 17, host the Solar Backscatter Ultraviolet (SBUV) spectrometer that has the objective of monitoring ozone in the Earth's lower atmosphere. In its discrete operating mode, a diffuser screen is placed in front of the instrument's aperture in order to scatter solar MUV radiation near 280 nm into the instrument.

This solar spectral region contains both photospheric continuum and chromospheric line emissions. The chromospheric Mg II *h* and *k* lines at 279.56 and 280.27 nm, respectively, and the weakly varying photospheric wings or continuum longward and shortward of the core line emission, are operationally observed by the instrument. On the ground, the Mg II core-to-wing ratio is calculated between the variable lines and nearly non-varying wings. The result is a measure of chromospheric and some photospheric solar active region activity independent of instrument sensitivity change through time, is referred to as the Mg II core-to-wing ratio (cwr), and is provided daily by NOAA Space Environment Center (SEC) as described by Viereck, *et al*.[10]

The ratio is an especially good proxy for some solar FUV and EUV emissions. Our analysis has found that it can represent very well the photospheric and lower chromospheric solar FUV Schumann-Runge Continuum emission. We have taken the Mg II cwr and performed a linear regression with $F_{10.7}$ for the common time frame to derive the $M_{10.7}$ index that is the Mg II cwr reported in $F_{10.7}$ units. Equation 4 provides the calculation of $M_{10.7}$ based on the NOAA 16 SBUV Mg II cwr data. We use the daily index, with a 5-day lag as described in Bowman and Tobiska[4], over the common time frame as a proxy for E_{SRC} since the latter is not operationally available.

$$M_{10.7} = (-1943.85) + (7606.56) \times Mg\_II_{NOAA16} \quad (4)$$

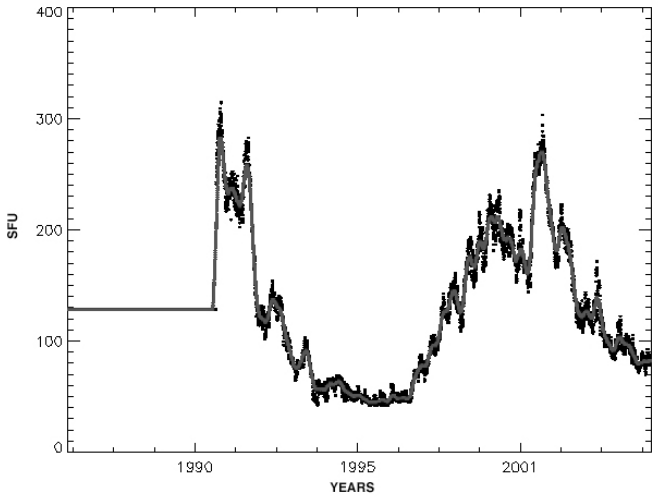

Fig. 5. $XL_{10.7}$ shown from 1991 into 2005 in sfu in black and the 81-day centered smooth shown in dark gray.

$XL_{10.7}$: The X-ray Spectrometer (XRS) instrument is part of the instrument package on the GOES series operational spacecraft. The XRS on GOES 10 and GOES 12 provide the 0.1–0.8 nm solar X-ray emission with 1-minute cadence and 5-minute latency. These data, used for flare detection, are continuously reported by NOAA SEC at the website of http://www.sec.noaa.gov/.

X-rays in the 0.1–0.8 nm range come from the cool and hot corona and are typically a combination of both very bright solar active region background that varies slowly (days to months) plus flares that vary rapidly (minutes to hours), respectively. The photons arriving at Earth are primarily absorbed in the mesosphere and lower thermosphere (80–90 km) by molecular oxygen and nitrogen where they ionize those neutral constituents to create the ionospheric D-region.

An index of the solar X-ray active region background, without the flare component, has been developed for operational use by Tobiska and Bouwer[11]. This is called the X_{b10} index and is used to represent the daily energy that is deposited into the mesosphere and lower thermosphere.

The 0.1-0.8 nm X-rays are a major energy source in these atmospheric regions during high solar activity but relinquish their dominance to the competing hydrogen (H) Lyman-α emission during moderate and low solar activity. Lyman-α is also deposited in the same atmospheric regions, is created in the solar upper chromosphere and transition region, and demarcates the EUV from the FUV spectral regions. It is formed primarily in solar active regions, plage, and network; the photons, arriving at Earth, are absorbed in the mesosphere and lower thermosphere where they dissociate nitric oxide (NO) and participate in water (H_2O) chemistry. Lyman-α has been observed by the SOLSTICE instrument on the UARS and SORCE NASA research satellites as well as by the SEE instrument on NASA TIMED research satellite as reported by Woods, *et al*.[12]

Since these two solar emissions are competing drivers to the mesosphere and lower thermosphere, we have developed a mixed solar index of the X_{b10} and Lyman-α (Lyα). It is weighted to reflect mostly X_{b10} during solar maximum and to reflect mostly Lyman-α during moderate and low solar activity. The independent, normalized F_{81} (81-day centered smoothed $F_{10.7}$ divided by the common time frame mean value, i.e., $F_{81\text{-normalized}}$) is used as the weighting function and multiplied with the X_{b10} and Lyman-α as fractions to their solar maximum values. Equation

5 provides the $XL_{10.7}$ index reported in sfu. We tested this daily index with an 8-day lag over the common time frame and found that it provides a few percent improvement in reducing the JB2006[3] modeled residuals versus the derived satellite densities. However, due to the operational complexity of producing this index, we decided not to include it in the final formulation of JB2006[3]. Figure 5 shows the $XL_{10.7}$ and the XL_{81} values from 1991 into 2005.

$$XL_{10.7} = \{F_{81\text{-normalized}} \times (X_{b10}/X_{b10\text{-max}}) + (1 - F_{81\text{-normalized}}) \times (Ly\alpha/Ly\alpha_{max})\} \times F_{81} \quad (5)$$

Forecasting Solar Indices and Proxies

The $F_{10.7}$, $S_{10.7}$, and $M_{10.7}$ proxies and indices, along with their 81-day centered smoothed values, are used as the solar inputs for the JB2006[3] empirical thermospheric density model. An additional motivation has been to provide real-time and forecast solar indices for thermospheric density and ionospheric applications. Space Environment Technologies (SET) has developed forecast algorithms to provides these three indices through the hybrid (empirical, physics-based, and data assimilative) SOLAR2000[13,14,15] (S2K) model and we report on those forecasts here.

SET uses 7 operational forecasting principles to produce the $F_{10.7}$, $S_{10.7}$, and $M_{10.7}$ solar indices and proxies:

1) time domain definitions of past, present, and future are clearly demarcated with identifiable granularity, cadences, and latencies starting with recognition of the current epoch;
2) information redundancy is clearly established using multiple data streams;
3) data reliability is guaranteed when quality forecasts flow uninterruptedly even with subsystem anomalies;
4) system robustness is achieved when an operational forecasting system is modular, manageable, and extensible using tiered architecture;
5) Technology Readiness Levels define the evolution of models and data to achieve system-level maturity;
6) geophysical validation is achieved if the output forecast represents the geophysical conditions within specified limits; and
7) operational verification is achieved if the output forecast meets the user-specified requirements' intent.

The foundation for the empirical forecasting in SET's Forecast Generation 2 (FGen2/D3.5) is persistence and recurrence and this is achieved using linear prediction for $F_{10.7}$, $S_{10.7}$, and $M_{10.7}$. We developed and tested a combination of algorithms based on SOHO/EIT 30.4 nm image analysis, including limb and center of disk data for active regions, plage, network, and background, as well as singular value decomposition routines coupled with empirical long-term active region evolution functions. However, in the 0–72 hours time frame, the Equation 6 generic formulation of a linear predictive technique proved to be most successful,

$$x_t = \varphi_1 x_{t-1} + \varphi_2 x_{t-2} \ldots + \varphi_P x_{t-P} + w_t \quad (6)$$

where x is the solar index value at a forecast time, t, P is most recent values to be used, φ are linear coefficients, and w is a residual error term. Out to 48 hours prediction we used the 3 most recent days of index values. Between 48–96 hours we used the last 5 solar rotations (137 days) as the most recent values. Our predictive results for high solar activity between January 20 and July 15 2001 are shown in figures 6, 7, and 8 for the $F_{10.7}$, $S_{10.7}$, and $M_{10.7}$ indices and proxies. Our results for low solar activity between April 1 and October 1 2005 are shown in figures 9, 10, and 11 for the $F_{10.7}$, $S_{10.7}$, and $M_{10.7}$ indices and proxies. Table C summarizes the regression coefficients from our forecasts for both high (2001) and low (2005) solar activity. The forecasts were generated every 6 hours throughout the six month duration of each solar activity period. There is a 3-hour time granularity at each forecast epoch.

We note that the nowcast correlation coefficients are not identically 1.0000 in Table C. This is because a nowcast at the current, 0 hour epoch is a forecast. Operational data come in asynchronously during the preceding nowcast time interval defined by SET as -24 hours to current epoch 0 hours. Since solar indices that are produced operationally are derived from multiple data sets, there is a time lag between the most recent values driving the forecast and the current epoch. In some cases, there may be a 24-hour lag between the current epoch nowcast and the most recent data used to create it. As a result, the correlation coefficients at the nowcast epoch are not 1.00000. The forecasts listed in Table C are exactly that. Future measurements have not yet arrived so the FGen2 algorithms make an estimate or prediction of solar indices and proxies at 3-hour intervals into the future out to 96-hours. We show "snapshots" of the correlation coefficients at 24-, 48-, 72-, and 96-hours in Table C and in the following figures.

Table C. Correlation coefficients (R) of forecast solar indices and proxies

Index or proxy	2001 nowcast	2001 24-hour	2001 48-hour	2001 72-hour	2001 96-hour	2005 nowcast	2005 24-hour	2005 48-hour	2005 72-hour	2005 96-hour
$F_{10.7}$	0.989090	0.982714	0.952312	0.904031	0.680845	0.983788	0.982915	0.944163	0.877398	0.596609
$S_{10.7}$	0.991434	0.986761	0.962630	0.911422	0.683100	0.981661	0.982107	0.945225	0.867663	0.626203
$M_{10.7}$	0.990299	0.987867	0.953183	0.894666	0.626743	0.988092	0.989048	0.955103	0.895198	0.727505

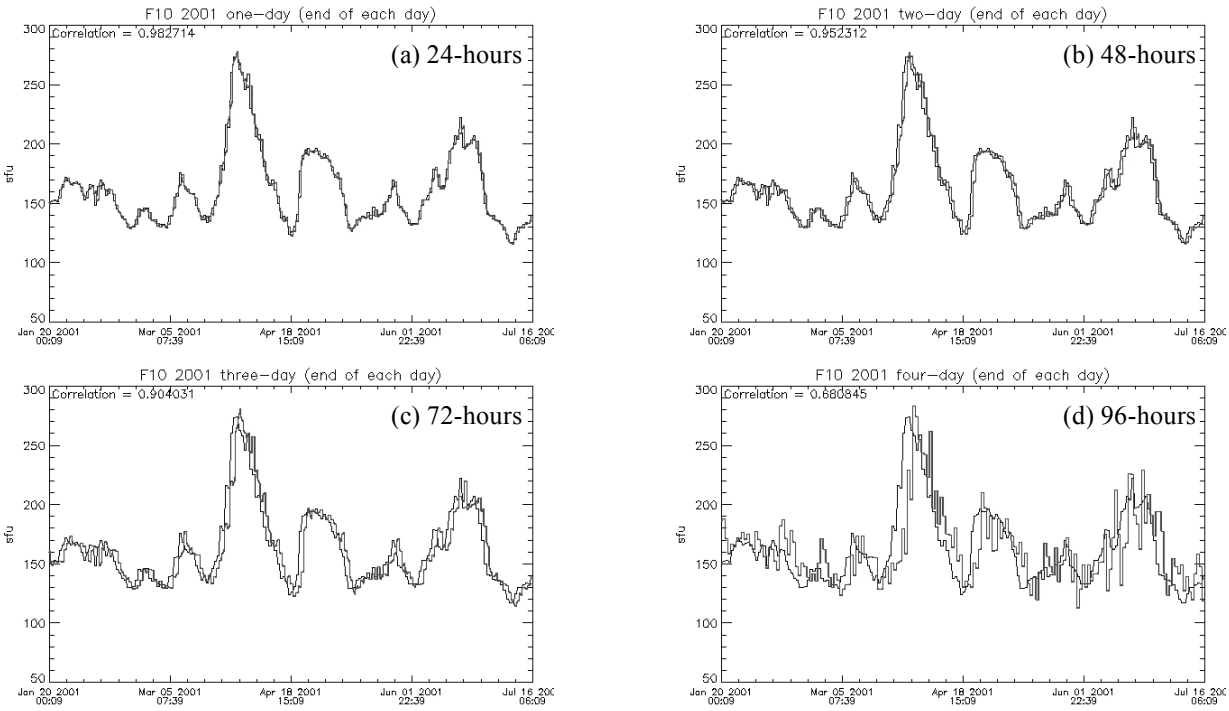

Figs. 6. Predicted (dark gray) and actual (black) $F_{10.7}$, with correlation coefficients [R], for January 20 – July 15 2001 at (a) 24-hours [0.982714], (b) 48-hours [0.952312], (c) 72-hours [0.904031], and (d) 96-hours [0.680845].

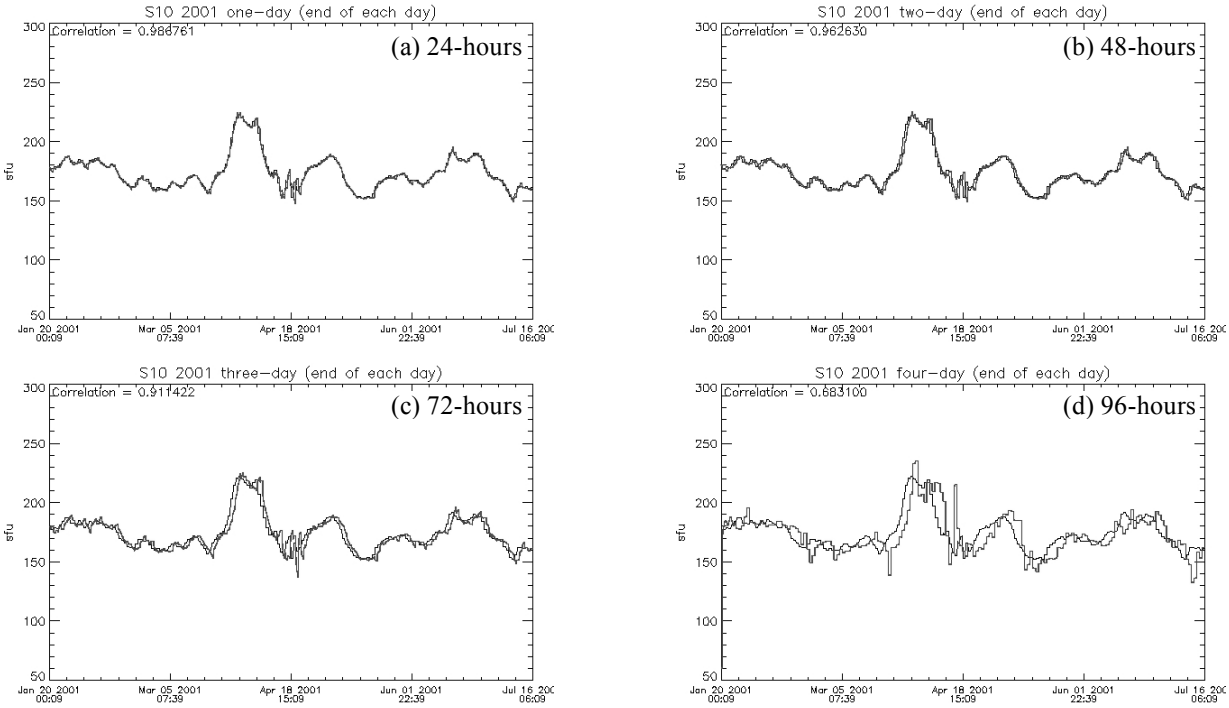

Figs. 7. Predicted (dark gray) and actual (black) $S_{10.7}$, with correlation coefficients [R], for January 20 – July 15 2001 at (a) 24-hours [0.986761], (b) 48-hours [0.962630], (c) 72-hours [0.911422], and (d) 96-hours [0.683100].

There has been substantial improvement in near-term forecasting over the past 5 years as evidenced in the above plots and Table C where most of the correlation coefficients are well above 0.90. To demonstrate the improvement through time, a comparison is useful between the 3-day forecasts of $F_{10.7}$ during the 2001 high solar activity test period. Three forecast results are shown: 1) NOAA SEC/Air Force Weather Agency (AFWA) that were

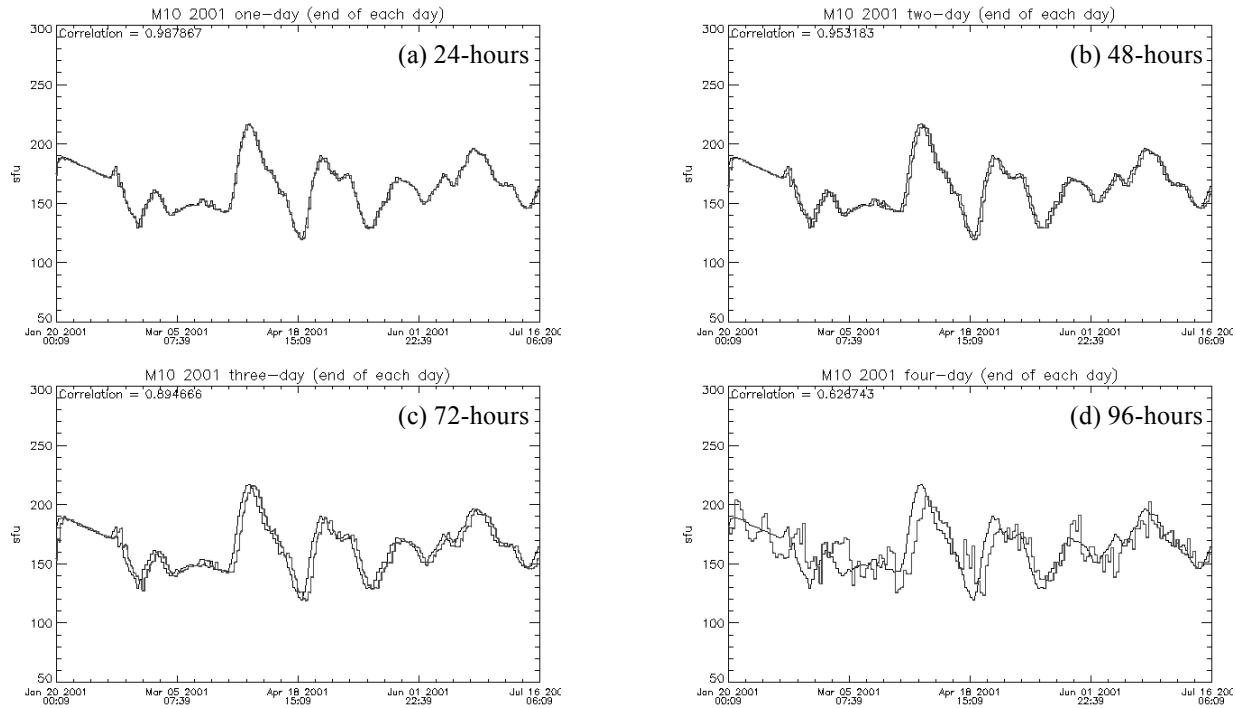

Figs. 8. Predicted (dark gray) and actual (black) $M_{10.7}$, with correlation coefficients [R], for January 20 – July 15 2001 at (a) 24-hours [0.987867], (b) 48-hours [0.953183], (c) 72-hours [0.894666], and (d) 96-hours [0.626743].

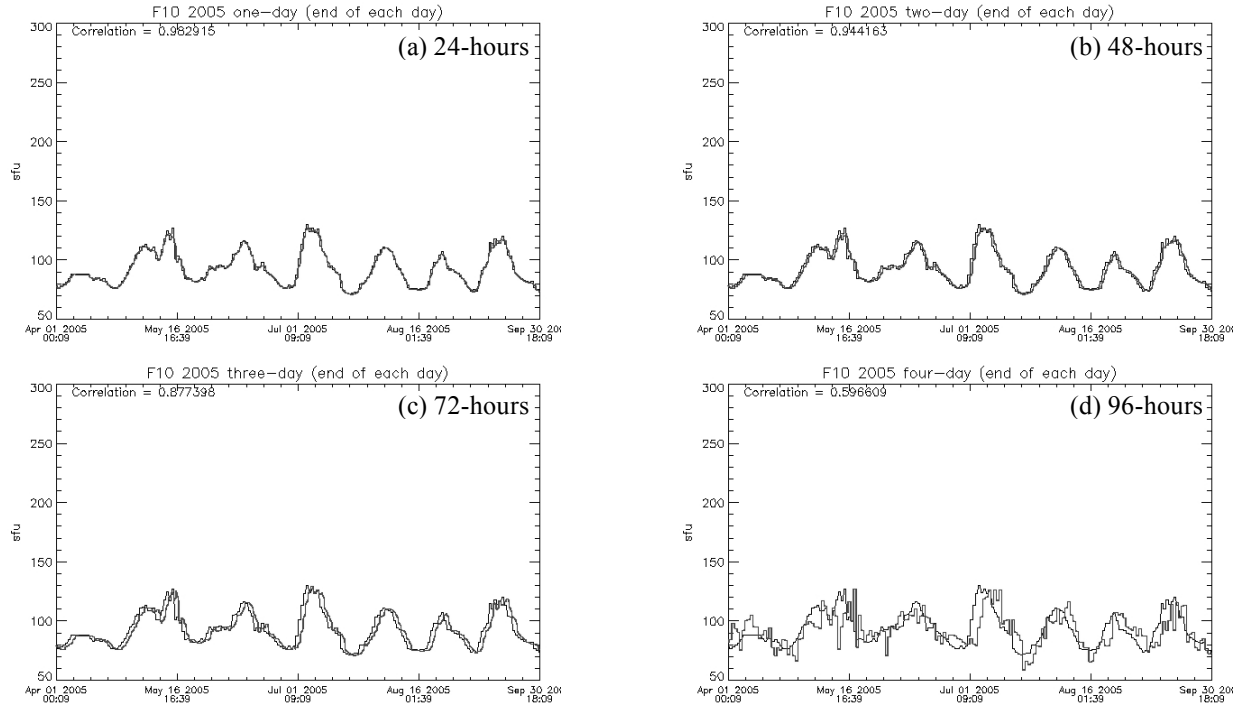

Figs. 9. Predicted (dark gray) and actual (black) $F_{10.7}$, with correlation coefficients [R], for April 1 – September 30 2005 at (a) 24-hours [0.982915], (b) 48-hours [0.944163], (c) 72-hours [0.877398], and (d) 96-hours [0.596609].

state-of-the-art in 2001, 2) SET's (HASDM) fully operational (TRL 9) FGen1x forecasts in 2003, and 3) SET's FGen2 prototype operational (TRL 7) forecasts (2006). Figure 12 graphically shows the improvement in which the forecasts at the 24-, 48-, and 72-hour epochs reduced every algorithm update cycle. Table D shows the 1-sigma % uncertainty for the NOAA SEC/AFWA, SET FGen1X (HASDM), and SET FGen2 algorithm updates.

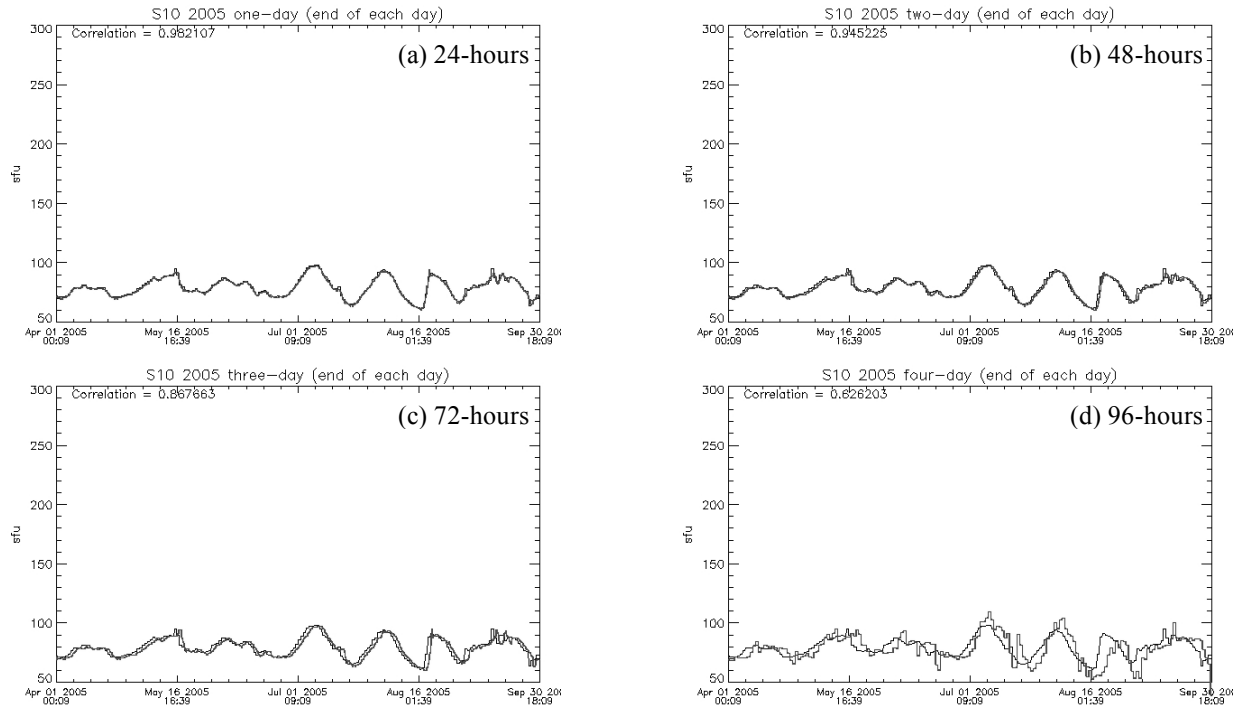

Figs. 10. Predicted (dark gray) and actual (black) $S_{10.7}$, with correlation coefficients [R], for April 1 – September 30 2005 at (a) 24-hours [0.982107], (b) 48-hours [0.945225], (c) 72-hours [0.867663], and (d) 96-hours [0.626203].

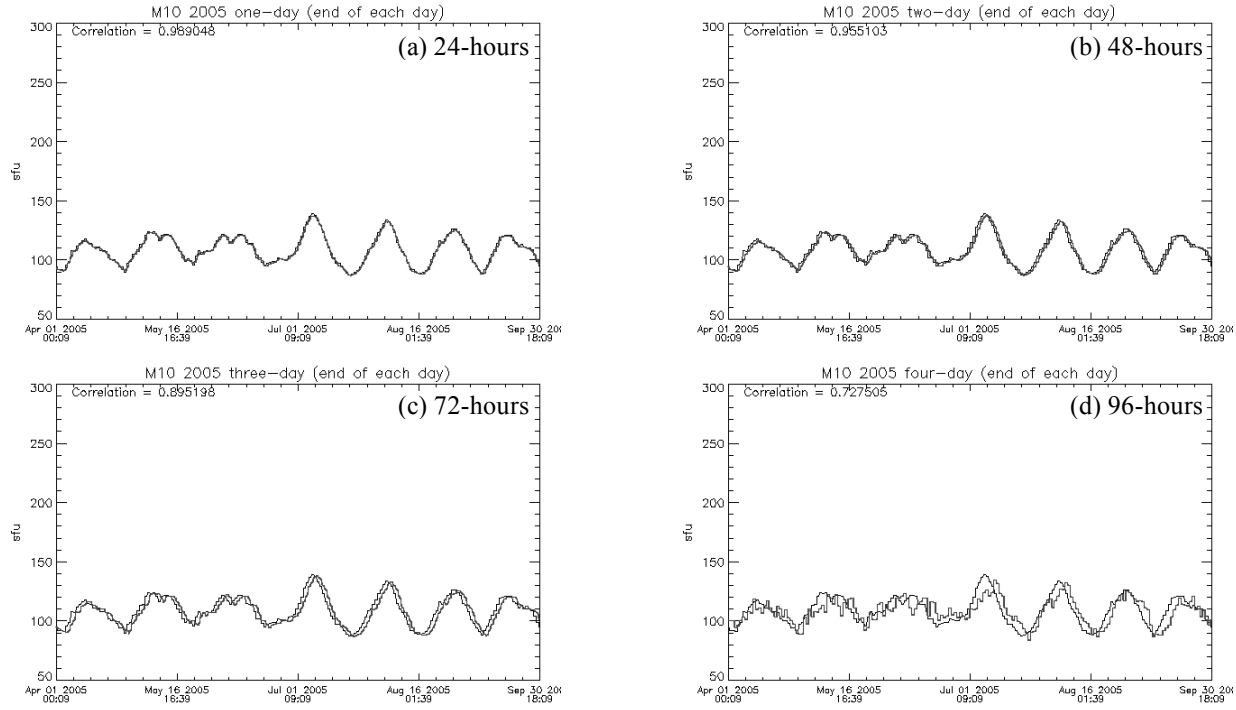

Figs. 11. Predicted (dark gray) and actual (black) $M_{10.7}$, with correlation coefficients [R], for April 1 – September 30 2005 at (a) 24-hours [0.989048], (b) 48-hours [0.955103], (c) 72-hours [0.895198], and (d) 96-hours [0.727505].

Conclusion

Our objective of providing an operational, system-level capability that reduces risk from space weather phenomena related to irradiance variability of energetic solar photons and their heating/ionization of the upper atmos-

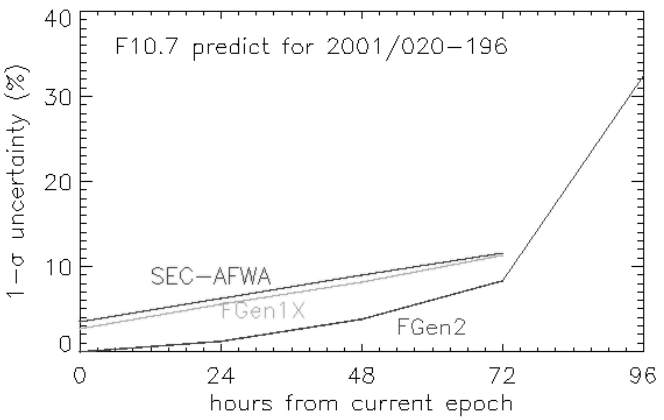

Fig. 12. $F_{10.7}$ 1-sigma percentage uncertainty in predictions by NOAA SEC/AFWA (top line), SET FGen1X (light gray middle line), and SET FGen2 (lowest dark line extending to 96 hours) every 3 hours from January 20 to July 15 in 2001.

phere has obtained significant success over the past 5 years. Our FGen2 linked data and model system is at TRL 7, i.e., a system prototype has been demonstrated in a relevant operational environment; the system is at or near the scale of an operational system with most functions available for demonstration and test; it is well integrated with collateral and ancillary systems and there is limited documentation available. It is designed to address the SSA challenges of *making measurements rapidly*, *interpreting them quickly*, and *reacting to the real-time and predicted information with appropriate and timely actions*.

Our current capabilities now combine real-time solar irradiance data streams with operational models to produce current epoch and forecast geoeffective integrated solar irradiances in the form of $F_{10.7}$, $S_{10.7}$, and $M_{10.7}$ indices and proxies. The $F_{10.7}$ proxy has existed for many years and, with a 1-day lag, continues to be a useful surrogate for cool corona and transition region XUV–EUV solar irradiances depositing their energy throughout the thermosphere. The new $S_{10.7}$ index of chromospheric EUV solar irradiances, with a 1-day lag, significantly improves the estimation of the solar energy that heats atomic oxygen in the terrestrial thermosphere. The revised $M_{10.7}$ proxy for photosphere/lower chromosphere FUV solar irradiances, based on the Mg II cwr and with a 5-day lag, significantly improves the estimation of the solar energy that dissociates molecular oxygen in the terrestrial lower thermosphere. One-sigma forecast uncertainties out to 72-hours are 1–10% for all three proxies/indices in high as well as low solar activity conditions. These three indices and proxies are designed for use in the new JB2006[3] thermospheric density model. They provide a significantly improved 72-hour thermospheric density forecast for operational satellite users and make available the information to interpret irradiance-related space weather events quickly and to react appropriately.

Table D. 1-sigma percentage uncertainty at selected forecast epochs

Hours from current epoch	+00	+24	+48	+72	+96
NOAA SEC/AFWA	3.6	6.3	9.0	11.7	–
FGen1X	2.7	5.6	8.2	11.4	–
FGen2	0.0	1.3	3.9	8.4	32.5

Acknowledgments

Support for this work has been provided by the contract GS-23F-0195N order delivery FA2550-06-F-8001. The leadership provided by the U.S. Air Force Space Battlelab with its Sapphire Dragon Initiative has provided the organizational foundation for the breakthroughs in this work. We thank Tom Woods and the UCB/LASP instrument teams for graciously providing UARS/SOLSTICE, TIMED/SEE, SORCE/SOLSTICE data. We thank Darrell Judge and Andrew Jones of the USC/SSC SOHO/SEM team for graciously providing SEM data. The historical indices described here for input to the JB2006 model are provided by SET at http://sol.spacenvironment.net/~jb2006/.

References

[1]ISO 21348, Space Environment (natural and artificial) – Process for determining solar irradiances, International Standards Organization (ISO), Geneva, 2006.

[2]COSPAR International Reference Atmosphere 1972 (CIRA72), compiled by the COSPAR Working Group IV, North-Holland Publishing Co., Amsterdam, 1972.

[3]Bowman, B.R. W.K. Tobiska, and F.A. Marcos, "A New Empirical Thermospheric Density Model JB2006 Using New Solar Indices", AIAA 2006-6166, 2006.

[4]Bowman, B.R. and W.K. Tobiska, "Improvements in Modeling Thermospheric Densities Using New EUV and FUV Solar Indices", AAS 06-237, 2006.

[5]Covington, A.E., Solar noise observations on 10.7 centimeters, *Proc. of the I.R.E.,* **36,** 454, 1948.

[6]Judge, D.L., H.S. Ogawa, D.R. McMullin, P. Gangopadhyay, and J.M. Pap, The SOHO CELIAS/SEM EUV Database from SC23 Minimum to the Present, *Adv. Space Res.,* **29** (12), 1963, 2001.
[7]Rottman, G.J. and T.N. Woods, The UARS SOLSTICE, *SPIE Proc.*, **2266**, 317, 1994.
[8]McClintock, W.E., G.J. Rottman, and T.N. Woods, SOLar Stellar Irradiance Comparison Experiment II (SOLSTICE II) for the NASA Earth Observing System's Solar Radiation and Climate Experiment Mission, *SPIE Proc.*, **4135,** 225, 2000.
[9]Woods, T.N., G.J. Rottman, R.G. Roble, O.R. White, S.C. Solomon, G.M. Lawrence, J. Lean, and W.K. Tobiska, TIMED Solar EUV Experiment, *SPIE Proc.,* **2266,** 467, 1994.
[10]Viereck, R., L. Puga, D. McMullin, D. Judge, M. Weber, W.K. Tobiska, The Mg II Index: A Proxy for Solar EUV, *Geophys. Res. Lett.,* **28** (7), 1342, 2001.
[11]Tobiska, W.K. and S.D. Bouwer, Solar flare evolution model for operational users, *2005 Ionospheric Effects Symposium,* ed. J.M. Goodman, JMG Associates, 76, 2005.
[12]Woods, T.N., W.K. Tobiska, G.J. Rottman, and J.R. Worden, Improved solar Lyman a irradiance modeling from 1947 through 1999 based on UARS observations, *J. Geophys. Res.*, **105,** 27195, 2000.
[13]Tobiska, W.K, T. Woods, F. Eparvier, R. Viereck, L. Floyd, D. Bouwer, G. Rottman, and O.R. White, "The SOLAR2000 empirical solar irradiance model and forecast tool," *J. Atm. Solar Terr. Phys.,* **62**, 1233-1250, 2000.
[14]Tobiska, W.K., "SOLAR2000 irradiances for climate change, aeronomy, and space system engineering," *Adv. Space Res.,* **34**, 1736-1746, 2004.
[15]Tobiska, W.K. and S.D. Bouwer, New developments in SOLAR2000 for space research and operations, *Adv. Space Research*, 37(2), 347-358, 2006, doi:10.1016/j.asr.2005.08.015.